

## Turbulence and jet-driven zonal flows: Secondary circulation in rotating fluids due to asymmetric forcing

M. J. Burin

*Department of Physics, California State University San Marcos, San Marcos, California 92096, USA*

K. J. Caspary

*Princeton Plasma Physics Laboratory, Princeton University, Princeton, New Jersey 08544, USA*

E. M. Edlund

*Department of Physics, State University of New York College at Cortland, Cortland, New York 13045, USA*

R. Ezeta

*Max Planck Center for Complex Fluid Dynamics, Mesa+ Institute, and J. M. Burgers Centre for Fluid Dynamics, University of Twente, P.O. Box 217, 7500AE Enschede, The Netherlands*

E. P. Gilson

*Princeton Plasma Physics Laboratory, Princeton University, Princeton, New Jersey 08544, USA*

H. Ji

*Department of Astrophysical Sciences and Princeton Plasma Physics Laboratory, Princeton University, Princeton, New Jersey 08544, USA*

M. McNulty

*Department of Mathematics, University of California Riverside, Riverside, California 92521, USA*

J. Squire

*Department of Physics, University of Otago, Dunedin 9016, New Zealand  
and Theoretical Astrophysics, California Institute of Technology, Pasadena, California 91125, USA*

G. R. Tynan

*Department of Mechanical Engineering and the Center for Energy Research, Jacobs School of Engineering, University of California, San Diego 92093, USA*



(Received 14 July 2018; published 12 February 2019)

We report on experiments and modeling on a rotating confined liquid that is forced by circumferential jets coaxial with the rotation axis, wherein system-scale secondary flows are observed to emerge. The jets are evenly divided in number between inlets and outlets and have zero net mass transport. For low forcing strengths the sign of this flow depends on the sign of a sloped end cap, which simulates a planetary  $\beta$  plane. For increased forcing strengths the secondary flow direction is insensitive to the slope sign, and instead appears to be dominated by an asymmetry in the forcing mechanism, namely, the difference in radial divergence between the inlet and outlet jet profiles. This asymmetry yields a net radial velocity that is affected by the Coriolis force, inducing secondary zonal flow.

DOI: [10.1103/PhysRevE.99.023108](https://doi.org/10.1103/PhysRevE.99.023108)

### I. INTRODUCTION

Zonal flows in rotating fluids, from Jovian atmospheric banding to the edge of tokamak plasmas, may emerge from smaller scales in a process of inverse energy transfer when the turbulent dynamics are essentially two dimensional (2D). This energy condensation was originally theorized via statistical arguments [1]. It has since been observed experimentally in flows that are effectively 2D due to rotation, stratification, magnetization, and actual thinness (e.g., soap films). This transfer or cascade of energy can

ultimately lead to large-scale self-organized flows, i.e., ones comparable to the system scale. Such a zonal flow, once formed, may in turn regulate the turbulence from whence it originated, e.g., in mitigating transport [2].

The inverse cascade of energy in 2D turbulence may be understood to be the spectral manifestation of vortex merging. However, energy transfer to larger scales can also occur through nonlocal interactions (via parametric or modulational instability), where a large-scale component emerges directly from small-scale interactions—understood vectorially as an acute resonant triad—due to the nonlinear advection of

vorticity, which is a common term in the analogous fluid equations describing both geostrophic fluids and magnetized plasmas [3]. There are thus at least two distinct routes to form large-scale structures from turbulence, even if the resulting zonal flows appear the same.

While the trend towards larger flow structures is a characteristic of 2D turbulence, turbulent energy may nevertheless fail to accumulate at the largest available scales due to competing processes. Recent theoretical work has sought to characterize conditions favorable to zonal jets, as opposed to a dominant central vortex [4]. One example incorporates wall friction [5], and another incorporates a spatially varying rotation frequency, e.g., a  $\beta$ -plane approximation, which is typically motivated by planetary-scale flows spanning latitudes. In this case the cascade process leads to an energy peak at the Rhines wave number  $k_R = (\beta/2U_{\text{rms}})^{1/2}$ , where  $U_{\text{rms}}$  is the rms velocity and  $\beta$  is the gradient of Coriolis frequency. Although defined for strictly barotropic flows, it is found that a variety of inhomogeneous natural zonal flows exist near the Rhines scale, including within Earth's oceans as well as the characteristic alternating bands seen on Jupiter [6].

In a laboratory setting, the gradient of Coriolis force with latitude may be approximated in a homogenous rotating fluid by setting up a potential vorticity gradient via sloped vertical boundaries. (Here the shallow end represents the planetary polar regions, and the deeper end represents the tropics.) Linearly sloped boundaries ensure a constant  $\beta$ , while allowing a free surface paraboloid yields a linearly increasing  $\beta$  with radius. In either case  $\beta = \frac{2\Omega}{h} \frac{dh}{dr}$ , where  $\bar{h}$  represents the mean fluid height,  $\Omega$  represents the rotation rate, and  $\frac{dh}{dr}$  represents the boundary gradient (i.e., slope). A number of previous experiments with this geophysical motivation in mind have used either or both of these boundary conditions to simulate a  $\beta$  effect.

The first laboratory study that observed a turbulence-driven zonal flow appears to be part of a larger work on source-sink flows by Hide [7]. In addition to flat boundaries, sloping boundaries of both signs were used, yielding mean flows in opposing directions, depending on the sign of the slope as expected. Further work by Whitehead, Jr. [8] made similar observations, and also investigated the saturation of the flow with increased forcing (in the form of a forcing-based Rossby number). The effect of turbulent forcing was also addressed [9,10], with Reynolds stresses estimated over radius from streak imaging. It was found that these stresses, and thus nonlinear interactions, peak slightly away from the forcing radius, where turbulent energy peaks, and somewhat outside of (but still close in radius to) where the mean flow is generated. The mean radial vorticity profile was found to be roughly linear and decreasing with radius. More contemporary experiments on zonal flow formation [11,12] have utilized particle image velocimetry (PIV) and have observed similar zonal flow production and vorticity distributions. Seminal large-scale experiments were performed on the Coriolis platform [13] in Grenoble, work that appears to be the first to estimate turbulent spectra. Wave-number spectra and their interpretation have been a prominent focus of subsequent  $\beta$ -plane experiments [14–16].

Of the experiments above some utilize jets coaxial with the rotation to create a turbulent background. This forcing

typically maintains zero net flux, i.e., mass flow via injection is equal to that from extraction. This may be accomplished with jets that carry flux in a unidirectional sense, in which case there are an equal number of inlets and outlets, or otherwise with each jet having an alternating flux (sloshing). In the former case all orifices are typically arranged to be at the same radius since separating inlets and outlets radially allows for the direct formation of zonal flow via Coriolis deflection of the mean radial flow between them [17].

The hydrodynamics of jets in confined vessels has been studied for some time, with applications found in various industries, including turbomachinery. But the focus has been primarily on mixing efficacy (of mass and heat) and not on particular flow patterns. Though the importance of eliminating “dead zones” (i.e., stagnant regions having little to no circulation) and the role of vessel geometry have been recognized as important, much of the more detailed work to date has focused on jet effects in a nonrotating working volume [e.g., 18].

In general, laboratory flow experiments with the intention of elucidating some phenomenon of larger-scale significance, for instance some geophysical and/or astrophysical flow phenomena, are typically subject to boundary conditions that have no natural analog. These practical limitations can complicate resulting data. In surveying previous laboratory work in this area, we note a lack of information regarding departures from ideal 2D expectations, for example, by reporting results of flows in the  $r$ - $\theta$  plane at only one axial location  $z$  with information at other  $z$  being unknown. Our results, described below, describe at least one type of nonideal effect that can occur when jet forcing is employed in a confined rotating fluid.

## II. LABORATORY APPARATUS

We have used a modified Taylor-Couette (TC) apparatus for the current experiments. The primary modification from a traditional TC device is split end caps, enabling better boundary layer controls to investigate bulk flow phenomena while mitigating the influence of boundary effects such as Ekman circulation [19]. The inner and outer radii ( $r_i$  and  $r_o$ ) are 6.9 and 20.3 cm, so the annular gap width  $d = 13.4$  cm and the radius ratio  $r_i/r_o = 0.34$ . The radially averaged aspect ratio is  $\bar{h}/d = 1.65$ ; due to a linearly sloped upper end cap, the vertical fluid column ranges from  $z = 20.95$  to 23.49 cm (measured from the vessel interior base) such that there is a height difference  $\Delta h$  corresponding to a  $10.7^\circ$  slope over  $d$ , with the average fluid height  $\bar{h} = 22.2$  cm (see Fig. 1). We employ two interchangeable end caps of opposite slopes, so that the values of  $h_i$  and  $h_o$  may be interchanged, allowing for  $\beta \pm 0.18$ . A flat upper surface ( $\beta = 0$ ) has also been employed as a control.

The outer cylinder and end-cap boundaries are made of cast acrylic for optical access, including for a laser Doppler velocimetry (LDV) diagnostic, which was mounted on a traverse below the rotating apparatus. The LDV system was calibrated using solid body rotation, revealing intrinsic noise levels of approximately 0.5–0.7%. This value includes minor mechanical noise due to rotation and diagnostic electronic noise as well as optical imperfections. Over the course of each run interior heating of the confined room-temperature water

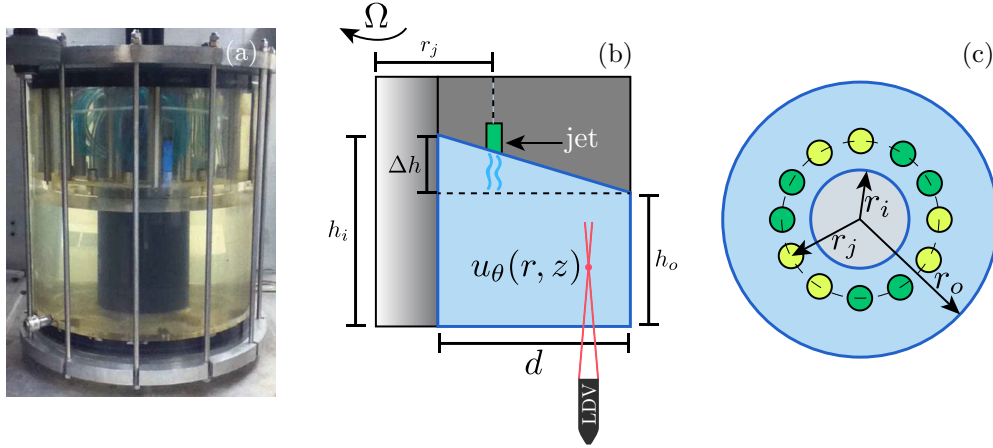


FIG. 1. Apparatus picture (a) and schematic views of the side (b) and top (c). At the inner and outer cylinder radii ( $r_i$  and  $r_o$ ) the fluid height varies ( $\Delta h$ ) due to a sloped end cap, the slope of which may be reversed to change the sign of  $\beta$ . The side schematic (b) includes a typical LDV diagnostic point, while the top view (c) pictures the forcing mode,  $m = 3$  with jets (centerline radius  $r_j = 12.45$  cm) paired, as in the experiment. Inlets for fluid extraction are shown in yellow (light gray) while outlets for fluid injection are shown in green (dark gray).

and thus consequent changes in viscosity were observed to be negligible (accurate to 0.5 C).

To focus on the phenomenon at hand in its most straightforward manifestation, we have used this vessel in simple solid body rotation, here at  $\Omega = 100$  rpm (10.5 rad/s), which for room-temperature water yields characteristic Ekman times of order  $\tau_{\text{Ek}} \sim \frac{\sqrt{d} \bar{h}}{\sqrt{\nu \Omega}} = 50$  s, where  $\nu$  is the kinematic viscosity. Typical experiments may be assigned a Reynolds number of  $\text{Re} = \frac{\bar{r} \Omega d}{\nu} \approx 2 \times 10^5$ , where  $\bar{r}$  represents the average radius, although the absence of any shear (including angular momentum gradients) in the background flow ensures stability despite the nominally high  $\text{Re}$ .

Forcing is provided by pumping through a circumferential array of 12 equally spaced and equally sized orifices in the upper boundary end cap (jet diameters are 0.95 cm; center radius  $r_j = 12.45$  cm). Fluid for all of the jets is pumped through a hollow central axle at rates  $Q \leq 840$  cm<sup>3</sup>/s. With all jets active in pumping—always six in, six out, but with different azimuthal mode numbers possible—this leads to jet velocities  $U_j$  up to about 2 m/s and  $\text{Re} \sim 19\,000$  based on orifice diameter. The forcing is unidirectional and coaxial and corotates with the bulk flow. For the experiments presented here,  $m = 3$  was used exclusively, as pictured in Fig. 1(c). Exploratory data using other  $m$  do not appear to differ significantly. We currently do not have direct imaging analysis or turbulent statistics of the jets themselves, but casual observation of occasional entrained bubbles suggests a turbulent exit.

### III. DATA AND DISCUSSION

Experiments were performed to investigate the dependence of secondary flows upon available control variables by obtaining radial profiles of the azimuthal velocity  $u_\theta$ , which are naturally averaged in  $\theta$  due to rotation. A typical run at each  $(z, r)$  location within the fluid is composed of a 4-min LDV time series: 1 min of data without forcing followed by 2 min with the jets turned on, followed by 1 min of decay and

quiescence. Between runs we allow several minutes to elapse, i.e., several  $\tau_{\text{Ek}}$ .

Figure 2(a) illustrates raw velocity data using this protocol, while Fig. 2(b) shows a departure from the solid body flow profile during the forcing period, indicating secondary mean flow. These departures from solid body rotation,  $\Delta u_\theta$ , are typically 0.01–0.1 m/s, so a maximum Rossby number for the induced flows,  $\text{Ro} = \frac{\Delta u}{2\Omega d}$ , is on the order of  $10^{-3}$ – $10^{-2}$ . Note that once the jets are turned off the background flow quickly loses turbulent energy, with a characteristic decay time near 5 s, which is roughly an order of magnitude less than  $\tau_{\text{Ek}}$ .

Our experimental results are summarized in Fig. 3, which gives radial profiles of  $\Delta u_\theta$  for our three values of  $\beta$  (−0.18, 0, and +0.18), for two jet forcing strengths ( $Q = 0.7$  and 5 gpm, or 44 and 315 cm<sup>3</sup>/s), and at four axial heights ( $z = 10.0$ , 13.4, 16.7, and 20.0 cm). Note that the lowest  $z$  given is slightly below the midplane. Profiles from the lower forcing and high  $z$  (15–20 cm, i.e., near the  $\beta$  plane) display the expected 2D result, with  $\pm\beta$  generating opposing weak zonal flows,  $+\beta$  being prograde over the forcing zone and retrograde outside it. The  $\beta = 0$  case by contrast generates no mean flow of significance. There is a clear departure from this pattern for higher forcing, however, in which case a large prograde (retrograde) flow is induced at high (low)  $z$ , irrespective of the sign of  $\beta$ .

We first discuss the  $\beta$ -dependent flows found with lower forcing. Whether turbulence-driven zonal flow(s) may be expected using the experimental parameters may be assessed in the following way. First, we should ideally have a clear scale separation between the smallest scale (turbulent forcing) and the largest ( $\bar{r}$  or  $d$ ), with the Rhines scale  $2\pi/k_{\text{Rh}}$  situated in between. Furthermore, the so-called zonostrophy index  $R_\beta = \frac{k_\beta}{k_{\text{Rh}}}$  should significantly exceed unity, where a transitional wave number  $k_\beta \approx (\frac{\beta^3}{\epsilon})^{1/5}$  ( $\epsilon$  being the energy transfer rate, estimated via dissipation  $\epsilon \approx \frac{U_{\text{rms}}^2}{2\tau_{\text{Ek}}}$ ). This index signifies that zonal flows should form on a timescale comparable to the characteristic eddy turnover time [13]. Using a typical

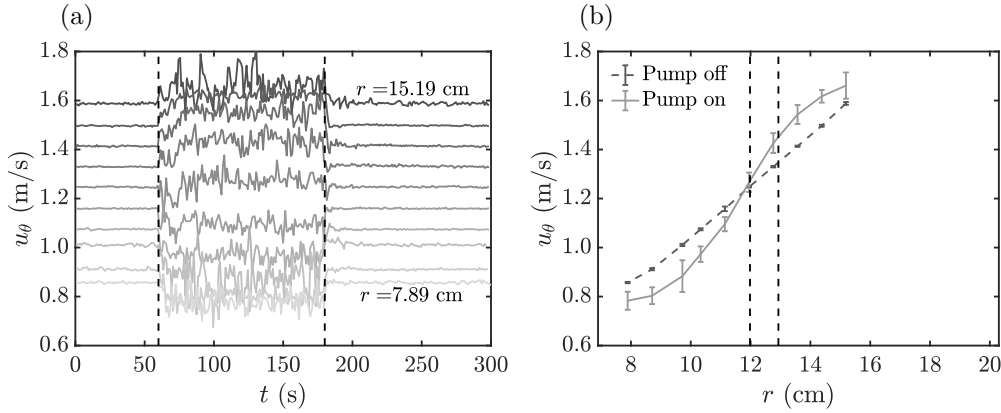


FIG. 2. (a) Raw velocity data for different radii, from smallest to largest ( $r = 7.89$  to  $15.19$  cm). The forcing pumps are active from 60 to 180 s. The intermediate radial locations may be seen on the abscissa of panel (b). (b) Solid body rotation is evident when the pumps are off (dashed line), but during forcing a departure from this profile due to secondary flow may be observed. Here  $\beta = -0.18$  and  $z = 19.4$  cm; these data are typical for  $z$  above the midplane. The vertical lines in panel (b) between 12 and 13 cm represent the inner and outer boundaries of the jets. Error bars represent one standard deviation.

$U_{rms} \sim 0.025$  m/s and  $\beta = 0.18$  we estimate  $R_\beta \approx 2.1$ . We find, however, that the Rhines scale exceeds 1 m, which is an

order of magnitude above the scale provided by the annulus. Thus while a zonal flow should be expected to form (i.e., temporally), it does not have the radial space to clearly do so. We note that previous experiments on turbulent-driven zonal flow formation have  $1 < R_\beta < 1.5$ , with a notable exception of  $R_\beta \approx 3.7$  being recently reported [16].

Our estimated value of  $R_\beta$ , however, must be taken with some caution for two reasons. First, we have measured only  $u_\theta$  fluctuations, and without matching fluctuations in radial velocity ( $u_r$ ) the total planar  $U_{rms}$  is not technically known, although similar experiments show them as comparable in magnitude [16], as might be expected [20]. Second, we have not disentangled the fluctuations of the 2D background flow from those intrinsic to the divergence of the three-dimensional (3D) jets. The data are limited in this respect since the induced flows are only found concomitant with active forcing.

We may account for the dynamical importance of background rotation compared to jet forcing with a transverse (to the plane of rotation) Rossby number,  $Ro_T = U_j/2\Omega h$ . For low forcing strengths  $Ro_T \sim 0.03$ , with the rms-based  $Ro$  being an order of magnitude smaller, while for the highest forcing  $Ro_T = 0.7$ , indicating that jet inertial effects are likely to be significant. We may also estimate the importance of 3D effects with an integral proxy, for example the volume replacement time,  $\tau_v = V/Q$ , which represents an essentially 3D process. For the flows in question to be dominantly 2D we should expect this time to far exceed the other dynamical timescales involved, especially the rotation period  $T$ . When we compare  $\tau_v/T$  for our smallest flow rate we find 345, a value comparable to 323 as found in [16]. Conversely our highest flow rate yields just 16, a value even lower than the value of 43 found in [11]. If we assume the condition  $\tau_v/T \gg 1$  needs to be met to ensure that 3D effects are insignificant in the background flow, then our higher forcing condition appears to be borderline. We note that  $\tau_v$  would not be a meaningful proxy for jets that switch inlet or outlet status periodically, as some experiments have done [12].

The secondary flows found at higher forcing, independent of  $\beta$ , are not of the same origin as the ones found at small forcing. We propose that these zonal flows are driven by

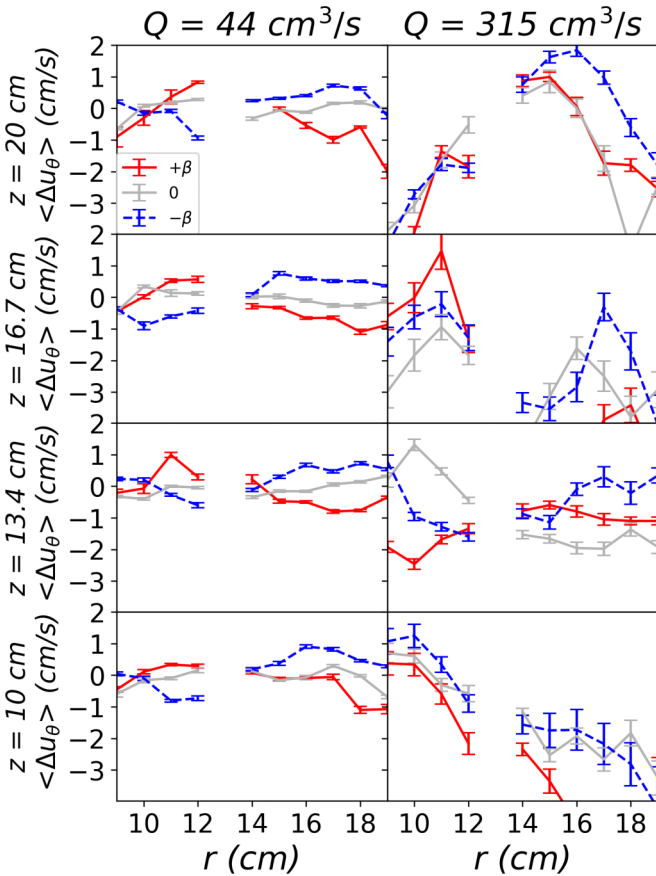


FIG. 3. Azimuthal velocity departures from solid body flow during forcing. Opposing zonal flows are observed with low forcing near the  $\beta$  plane with  $+\beta$  in red (dark gray) and  $-\beta$  in blue (dashed, black). The  $\beta = 0$  case is shown in light gray. Stronger and more height-dependent induced flows, which are independent of  $\beta$ , appear with higher forcing. All data are with  $m = 3$  and  $\Omega = 10.5$  rad/s. Data in line with the forcing jets have been removed for clarity.

jet divergence asymmetry, that is, the asymmetry of radial motions associated with entering and exiting the vessel via orifices. The latter (extraction from the vessel) typically has much stronger radial motions near the opening, at higher  $z$ . Conversely jet injection velocities typically display a positive divergence that is more gradual downstream (decreasing  $z$ ). At each  $z$ , the net difference between these radial motions under the influence of the Coriolis force should induce secondary azimuthal flows. Specifically, the dominant inlet convergence associated with fluid extraction should yield a prograde secondary flow near the forcing height for  $r > 12$  cm, as we observe. Furthermore, a retrograde flow is found below the midplane. This counterflow may be due to the more dominant divergence of the jets downstream, or perhaps originates just to conserve total angular momentum, as there is no net torque within the vessel due to the jets.

Given that the magnitude of the induced flow  $\Delta u_\theta$  is on the order of  $\sim 1\%$  of the jet velocity  $U_j$ , jet bias needs to be ruled out. For example, a slight tilt to the jets (only a couple degrees would be needed) was ruled out by simply reversing the sign of  $\Omega$ . Reversing the rotation also rules out azimuthal bias (i.e., tangential tilt) of the jet(s), while switching the inlet or outlet status of jets rules out radial bias. With direct means for the jets to drive the observed  $\beta$ -independent flows removed, a more indirect mechanism such as divergence asymmetry is required.

#### IV. NUMERICAL SIMULATIONS

The zonal flows seen at low forcing, affected by the  $\beta$  plane, have been (for our purposes) adequately simulated and characterized before [10,11]. To investigate the origin of the secondary flows seen in our data at larger forcing we have used the DEDALUS code [21], which provides a flexible framework for the solution of partial differential equations using a pseudospectral method with mixed Fourier-Chebyshev basis. With it we solve the standard incompressible Navier-Stokes equations in a frame rotating with angular velocity  $\Omega$  ( $z$ ):

$$\partial_t u + u \cdot \nabla u + 2\Omega \times u = -\nabla p + \nu \nabla^2 u. \quad (1)$$

The domain, which represents a cubic “patch” of the cylindrical working volume, has dimensions  $L_x \times L_y \times L_z = 9.5 \times 9.5 \times 9.5$  cm, with periodic boundary conditions in the azimuthal ( $\theta$ ) and radial ( $r$ ) directions, and no-slip boundary conditions at  $z \pm 9.5$  cm. We use a viscosity  $\nu \approx 5 \times 10^{-5} \text{ m}^2 \text{ s}^{-1}$ , which, although unphysically large (by a factor of about 50), is necessary to damp fluid motions above the grid scale and avoid spectral reflection issues. The grid has dimensions  $64 \times 64 \times 192$ . Pressure is solved for as a basic constraint to maintain flow incompressibility.

The jets are modeled with a Gaussian inflow or outflow condition on the upper  $z$  boundary:

$$u_z(x, y, L_z) = v_{\text{jet}} \exp\left[-\frac{x^2 + (y - L_y/4)^2}{w_{\text{jet}}^2}\right] - v_{\text{jet}} \exp\left[-\frac{x^2 + (y + L_y/4)^2}{w_{\text{jet}}^2}\right] \quad (2)$$

where  $v_{\text{jet}} = 0.75 \text{ cm/s}$  is the simulated jet strength, normally distributed and chosen to match the high-flow ( $Q = 315 \text{ cm}^3/\text{s}$ ) flow rate shown in Fig. 3, and  $w_{\text{jet}} = 0.57 \text{ cm}$  is the jet width, chosen such that the Gaussian profile has a width that approximately matches the 0.95-cm jet diameter of the experiment. Note there was no system curvature in the simulation, so  $(x, y)$  represent  $(\theta, r)$ .

The jet boundary conditions (2) were gradually increased at the start of the simulation ( $v_{\text{jet}} = 0$  at  $t = 0$ ), reaching their full magnitude at  $t = 1$ , so as to avoid an impulsive start to the system. We ran a suite of simulations, varying  $\Omega$  from 20 to 1000 rpm. (One could alternately consider  $\Omega$  to be fixed, while the jet strength is varied.) We emphasize that these simulations, rather than providing a detailed model of the experiment, are intended primarily to validate the secondary flow generation mechanism discussed above. Due to numerical issues caused by the sharp gradients in the boundary conditions of the jet, as well as limitations on available computational resources (and thus the achievable Re), we were unable to numerically reach the regime where the jets become truly turbulent. The simulations thus provide some confirmation of the validity of the divergence-asymmetry forcing mechanism discussed above, but they cannot be quantitatively compared to the experimental results.

Results from the simulations are seen in Fig. 4, where secondary zonal flows are seen to develop even though  $\beta = 0$ . An identical simulation with the zero Coriolis term ( $\Omega = 0$ ) fails to develop these jet-driven flows. As in the data, a counterflow is observed in the simulations at lower  $z$ , i.e., farther from the orifices. Whether this counterflow is due to the increased net divergence of the flow at greater downstream distance, or due to momentum conservation in the absence of net torque, is not known. Its presence, direction, and magnitude are sensitive to both background rotation ( $\Omega$ ) and jet flux ( $Q$ ), as well as the box dimensions and the viscosity. Additional simulations with a more realistic viscosity are needed to better characterize its axial structure.

Figure 4(b) shows results exploring the role of background rotation on these simulated secondary flows, demonstrating an increasing constriction of the jets with increasing  $\Omega$ , especially for extraction, which sharpens considerably with  $\Omega$ , while the effect on the injected jet profile is less notable. Note that the area under each profile curve is constant, reflecting zero net flux as is required for a constant and incompressible working volume. The trend of increasing confinement with  $\Omega$  can be understood considering the Taylor-Proudman theorem, which would prohibit vertical variation of radial motions for  $\Omega \rightarrow \infty$  (or  $\nu \rightarrow 0$ ). Figure 4(c) shows the joint effect of the jet confinement, or decreased divergence, concomitant with the Coriolis force that deflects the net radial velocity component to induce azimuthal flow. The mechanism is thus understood to arise from a competition of two effects that both strengthen with rotation: the reduction of vertical variation of radial motions (Taylor-Proudman) and the enhanced secondary flow from these radial motions (Coriolis).

The maximum magnitude of this induced flow varies as  $\max\{u_\theta\} \propto \Omega^{2/3}$ , where  $\max\{u_\theta\}$  represents the largest deviation from solid body flow. The scaling exponent may be decomposed to be  $1 - \eta$ , where 1 represents the linear Coriolis term and  $\eta$  represents the competing effect of the jet

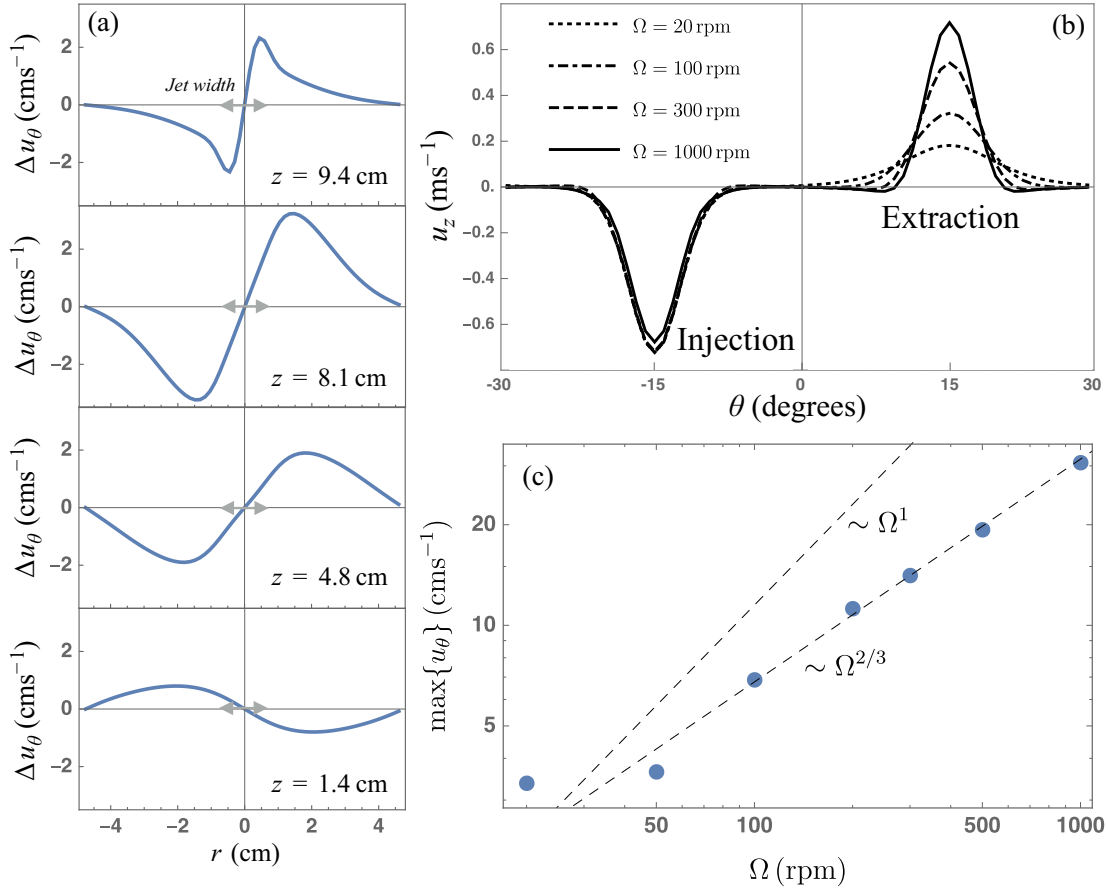


FIG. 4. Simulation results on zonal flows due to jet asymmetry with  $\beta = 0$ . (a) Azimuthal velocity difference, averaged over the azimuthal direction, for the scaled-down  $\Omega = 50$ -rpm simulation, demonstrating a prograde flow for  $r > 0$  near the orifices, driven by the stronger radial motions associated with fluid extraction. A retrograde flow is found well below the midplane (here at  $z = 4.75$  cm); note that the axial profile is sensitive to both  $\Omega$  and  $v$ . (b) Jet outflow/inflow radial profiles of axial velocity  $u_z(\theta)$  and their narrowing with  $\Omega$ , especially for extraction. The area under each curve remains constant, reflecting zero net flux. (c) Joint effect of rotation upon the secondary flow maximum magnitude,  $\max\{u_\theta\}$ , yielding an approximate  $2/3$  power law scaling as described in the text.

constriction under rotation. Consequently we find  $\eta = 1/3$ , although we emphasize again that it may be different at lower viscosities when the jets are turbulent. In fact, there seems to be no reason why  $\eta$  cannot exceed unity, so that increased rotation suppresses these induced flows. Indeed, in exploratory higher- $\Omega$  simulations and experiments the secondary flow appears to be much reduced. Nevertheless, we note a similarity of this  $1/3$  scaling to those associated with free-shear layers in rotating flows, namely, for the inner core of (coaxial) Stewartson layers responsible for vertical mass transport [22]. Future theoretical work is needed to provide details on this potential analogy, and on the nature of  $\eta$ , especially for turbulent regimes.

V. SUMMARY AND FUTURE WORK

In this paper we have presented results that document two distinct types of secondary flows, one originating from turbulence and affected by the  $\beta$  plane and the other due to an asymmetry in the forcing mechanism, namely, a difference between injection and extraction jet profiles, which yields a net radial divergence that is affected by the Coriolis force, inducing secondary zonal flow. These jet-driven flows

depend on axial location ( $z$ ) and also vary nontrivially with background rotation: while Coriolis deflection increases with  $\Omega$ , concomitantly jet profiles are constricted with their radial velocities reduced, so that the two effects are essentially in competition.

The turbulence-driven  $\beta$ -plane zonal flow discussed initially has been observed before, being usually motivated by geophysical questions, but typically with little documented exploration of nonideal or 3D boundary effects that are common to experimentation using confined laboratory flows. By contrast, we can find no documented reference to the jet-driven secondary flow in the literature. Nevertheless, these flows seem likely to be common. There have been studies that investigate the consequences of Coriolis deflection of a jet within a rotating duct [23], but none to date apparently account for the deflection of the jet divergence. This, along with the  $\Omega^{1/3}$  scaling similarity found in Stewartson layers, suggests a potentially fruitful direction for future work. The significance of this jet-driven secondary flow should at least be considered in experiments using rotating fluids and jets to produce turbulence-driven zonal flows. We note that, while not explicitly stated, techniques such as alternating the jet flux direction [12] and using smaller diameter orifices for

extraction [16] are employed presumably to avoid these secondary flows, just as De Verdier employed a layer of foam rubber near the forcing “to avoid jetting effects at the mouth of the tubes” [9].

Additional directions for future work on this topic would do well to include a focus on which flow geometries and background flow regimes favor which secondary flows. In addition to the forcing magnitude ( $Q$  or jet  $Re$ ) and the orifice diameter distribution,  $\Omega$ ,  $\beta$ , and vessel axial height  $h(r)$  are typically accessible variables that may be altered experimentally. An examination of forcing spatial scale as a control variable could also be interesting and potentially useful: exploring different azimuthal mode numbers ( $m$ ) as well as varying the wavelength of the low-order  $m$ , that is, to produce  $m = 1, 2$ , and  $3$  using different numbers of contiguous jets. Additional diagnostics should prove worthwhile as

well, for example by complementing LDV with PIV, allowing for coherent structures and spectra to be discerned. Additional simulations at higher  $Re$  and further theoretical work should also be pursued so that the structure and relative magnitudes of the two types of secondary zonal flows may be more thoroughly and quantitatively compared.

#### ACKNOWLEDGMENTS

We thank P. Slobota [Princeton Plasma Physics Laboratory (PPPL)] for extensive hardware work as well as P. Dang for helping with initial data collection; initial theoretical discussions with T. Stoltzfus-Dueck (PPPL) were also valuable. M.J.B. recognizes sabbatical support provided by PPPL and the former U.S. Department of Energy Center for Momentum Transport and Flow Organization.

- 
- [1] R. H. Kraichnan, Inertial ranges in two-dimensional turbulence, *Phys. Fluids* **10**, 1417 (1967).
- [2] P. W. Terry, Does flow shear suppress turbulence in nonionized flows? *Phys. Plasmas* **7**, 1653 (2000); M. G. Shats, H. Xia, H. Punzmann, and G. Falkovich, Suppression of Turbulence by Self-Generated and Imposed Mean Flows, *Phys. Rev. Lett.* **99**, 164502 (2007).
- [3] A. I. Smolyakov, P. H. Diamond, and V. I. Shevchenko, Zonal flow generation by parametric instability in magnetized plasmas and geostrophic fluids, *Phys. Plasmas* **7**, 1349 (2000); C. Connaughton, B. T. Nadiga, S. Nazarenko, and B. E. Quinn, Modulational instability of Rossby and drift waves and generation of zonal jets, *J. Fluid Mech.* **654**, 207 (2010).
- [4] A. Frishman, J. Laurie, and G. Falkovich, Jets or vortices: What flows are generated by an inverse turbulent cascade? *Phys. Rev. Fluids* **2**, 032602-1 (2017).
- [5] S. Danilov and D. Gurarie, Rhines Scale and spectra of the  $\beta$ -plane turbulence with bottom drag, *Phys. Rev. E* **65**, 067301 (2002).
- [6] B. Galperin, H. Nakano, H.-P. Huang, and S. Sukoriansky, The ubiquitous zonal jets in the atmospheres of giant planets and Earth’s oceans, *GRL* **31**, L13303 (2004).
- [7] R. Hide, On source-sink flows in a rotating fluid, *J. Fluid Mech.* **32**, 737 (1968).
- [8] J. A. Whitehead, Jr., Mean flow generated by circulation on a beta-plane: An analogy with the moving frame experiment, *Tellus* **27**, 358 (1975).
- [9] A. C. De Verdier, Mean flow generation by topographic Rossby waves, *J. Fluid Mech.* **94**, 39 (1979).
- [10] A. D. McEwan, R. O. R. Y. Thompson, and R. A. Plumb, Mean flows driven by weak eddies in rotating systems, *J. Fluid Mech.* **99**, 655 (1980).
- [11] J. Aubert, S. Jung, and H. Swinney, Observations of zonal flow created by potential vorticity mixing in a rotating fluid, *Geophys. Res. Lett.* **29**, 23-1 (2002).
- [12] J. J. Rasmussen, O. E. Garcia, V. Naulin, A. H. Nielson, B. Stenum, L. J. A. van Bokhoven, and S. Delaux, Generation of zonal flows in rotating fluids and magnetized plasmas, *Phys. Scr.* **T122**, 44 (2006).
- [13] P. L. Read, Y. H. Yamazaki, S. R. Lewis, P. D. Williams, R. Wordsworth, K. Miki-Yamazaki, J. Sommeria, and H. Didelle, Dynamics of convectively driven banded jets in the laboratory, *J. Atmos. Sci.* **64**, 4031 (2007).
- [14] G. Di Nitto, S. Epsa, and A. Cenedese, Simulating zonation in geophysical flows by laboratory experiments, *Phys. Fluids* **25**, 086602 (2013).
- [15] P. Zhang and Y. D. Afanasyev, Beta-plane turbulence: Experiments with altimetry, *Phys. Fluids* **26**, 026602 (2014).
- [16] S. Cabanes, J. Aurnou, B. Favier, and M. Le Bars, A laboratory model for deep-seated jets on the gas giants, *Nat. Phys.* **13**, 387 (2017).
- [17] S. D. Meyers, J. Sommeria, and H. L. Swinney, Laboratory study of the dynamics of Jovian-type vortices, *Physica D* **37**, 515 (1989); E. Crespo del Arco, P. Maubert, A. Randriamampianina, and P. Bontoux, Spatio-temporal behaviour in a rotating annulus with a source-sink flow, *J. Fluid Mech.* **328**, 271 (1996).
- [18] H. D. Zughbi and M. A. Rakib, Mixing in a fluid jet agitated tank: Effects of jet angle and elevation and number of jets, *Chem. Eng. Sci.* **59**, 829 (2004); S. Jayanti, Hydrodynamics of jet mixing in vessels, *ibid.* **56**, 193 (2001).
- [19] M. J. Burin, H. Ji, E. Schartman, R. Cutler, P. Heitzenroeder, W. Liu, L. Morris, and S. Raftopolous, Reduction of Ekman circulation within Taylor-Couette flow, *Exp. Fluids* **40**, 962 (2006); E. M. Edlund and H. Ji, Nonlinear stability of laboratory quasi-Keplerian flows, *Phys. Rev. E* **89**, 021004(R) (2014).
- [20] A. Ibbetson and D. J. Tritton, Experiments on turbulence in a rotating fluid, *J. Fluid Mech.* **68**, 639 (1975).
- [21] <http://dedalus-project.org>.
- [22] H. P. Greenspan, *The Theory of Rotating Fluids* (Cambridge University, Cambridge, England, 1968).
- [23] S. K. Hong, D. H. Lee, and H. H. Cho, Effect of jet direction on heat/mass transfer of rotating impingement jet, *Appl. Therm. Eng.* **29**, 2914 (2009).